International Journal of Steel Structures 16(1): 73-89 (2016)
DOI 10.1007/s13296-016-3007-y
ISSN 1598-2351 (Print)
ISSN 2093-6311 (Online)

International Journal of
STEEL
STRUCTURES
www.springer.com/journal/13296

A Study to Enhance the Deformation Capacity of Beam-to-Column Connections Using High Strength Steel Having High Yield Ratio

Sang-Hoon Oh[1] and Hae-Yong Park[2,*]

[1]*Professor, Department of Architecture, Pusan National University, Busan, 609-735, Korea*
[2]*Ph.D. Student, Department of Architecture, Pusan National University, Busan, 609-735, Korea*

Abstract

As structures are becoming bigger and more having long span, construction materials are also becoming higher performance materials. In response to this trend, 800MPa tensile strength class structural steel was developed in South Korea. Currently, many experiments applied high strength steel about flexural members, compression members, and connections are continuously conducted, but the design guideline for high strength steel has yet to be established. From among these, it is more difficult that planning of ductile beam-to-column connections because of the high yield ratio, which is the characteristic of high strength steel and related studies are not sufficient. Therefore, This study proposed connection details for the purpose of enhancing the deformation capacity of high strength steel beam-to-column connections and it conducted full-scale experiment and FEM analysis using the connection detail as the variable. As the connection detail, it applied non-scallop welding method and improved horizontal stiffener construction method. Especially, it suggests the stress balance design formula for the improved horizontal stiffener construction method, in order to improve the efficacy of strain distribution. Through the results of experiment and FEM analysis, it was analyzed structural performance of connections with proposed details, and it suggested the design scope of the improved horizontal stiffener.

Keywords: high-strength steel, beam-to-column connection, deformation capacity, connection detail, yield ratio, improved horizontal stiffener

1. Introduction

There have been increasing interest in developing high performance materials in order to meet the needs of structures which are becoming bigger. In response to this trend, high strength steel A514 and A709 (yield strength: 690 MPa) were developed in the USA, and HT80 & H-SA700 (yield strength: 780 MPa) and HT100 (yield strength: 950 MPa) were developed in Japan. A high strength steel HSB800 (yield strength: 800 MPa) was developed in South Korea in 2009 for civil engineering and HSA800 having the same target tensile strength was also developed for construction. However, as has already been known, the high strength steel has the advantage of securing structure strength, but it is hard to secure stiffness and it may lower plastic deformation capacity and toughness of flexural member due to having a higher yield ratio and lower elongation percentage compared with general structural steel (mild steel). Especially, If high strength steel is applied to beam-to-column connections with complex stress mechanism, it is very likely to lower rotational capacity of connections due to the brittle tendency of the weld zone and the base metal. Diverse experiments have been conducted on applying high strength steel flexural members, but the deformation capacity of high strength steel connections from those experiment results is lower than the deformation capacity of general structural steel, and the range of application has yet to be expanded (McDermott, 1969; Galambos *et al*., 1997; Bjorhovde, 2004; SAC Joint Venture, 2000). Accordingly, application of high strength steel flexural member is strictly restricted around the world, and they are only applicable to some parts generating overload of short span beam members. However, it is clear that the high strength steel materials with excellent strength and elastic deformation compared with general steel is sufficiently attractive materials for constructors in the field and the researchers alike, and the continuous study aimed at overcoming weakness of high strength steel as well as developing new materials meets the trend of current construction market which requires higher performance.

Received May 7, 2015; accepted November 27, 2015;
published online March 31, 2016

*Corresponding author
Tel:+82-51-510-7608; Fax:+82-51-514-2230
E-mail:haeyong2610@hanmail.net

This study suggests connection details to improve deformation capacity of the connections for high strength steel (HSA800, target tensile strength: 800 MPa) and experimentally reviews the applicability of high strength steel flexural member with high yield ratio. In addition, an analytical model of high strength steel connections capable of comparing high strength steel connections with general structural steel connections and analyzing it across variables is drawn through nonlinear finite element analysis. An optimized design formula for suggested connection details is then suggested through additional variable analysis.

2. Deformation Capacity of Connections Depending on the Connection Details

The major factor responsible for lowering deformation capacity of high strength steel flexural member is the lack of toughness of material, and the high yield ratio (ratio of Yield Strength to Tensile Strength) of high strength steel is the factor directly responsible for lowering the toughness of material. The yield ratio is a mechanical characteristic and it is necessary to induce plastic hinge into the beam and dissipate the strain at the maximum stress point in order to improve deformation capacity of connections after the materials have been already selected. In particular, brittleness may be promoted at the heat-affected zone by the notch and martensite generated from the welding process, if the beam and the column are connected with rigid joint by welding. And when applying high strength steel, it's necessary to pay more attention to stress concentration in the outer side of column. At the moment, developing connection details which enables ductile behavior is the most probable alternative for resolving problems mentioned above. The concept of these connection details is hinted by the concepts of connection details developed by USA and Japan after two earthquakes in the 1990s', namely the Northridge earthquake (1994) and the Kobe earthquake (1995). Among them, Reduced Beam Section (RBS), one of the post north-ridge connection details suggested by FEMA350, haunched beam, and horizontal stiffener construction method contain the idea of Capacity Design Method as connection details designed to induce the location of plastic hinge into the inner area through section reinforcement or face cutting of the beam member (Chen, 2001; Engelhardt *et al*., 2000). In addition, in the case of Welded Unreinforced Flange-Welded Web (WUF-W) connection detail and Japan's Non-scallop connection detail are capable of relieving the stress concentration by improving and removing scallop (Oh *et al*., 2010). Performance verifications of these connections detail have been conducted by experimental studies targeting general structural steel, and they proved that the risk of brittle fracture occurring at the outer side of column can be reduced compared with Pre-Northridge connection detail, and excellent deformation capacity can be achieved (Uang and Bondad, 1996a,b; Sophianopoulos and Deri, 2011; Oh and Kim, 2008; Kim and Oh, 2008; Wang *et al*., 2010; Hu and Hwang, 2013). However, according to recent experiments (Fig. 1), RBS connection showed early lateral buckling on the cross-section crop and resultant decrease of the bearing force (Lee and Kim, 2007). In addition, there exists a concern that the horizontal stiffener construction method may cause unexpected brittle fracture at the stress concentration point when applying high strength steel with high yield ratio due to occurring stress concentration at the end of reinforcement. Therefore, this study will apply the qualified Non-scallop detail to relieve strain of outer side of column and apply a new construction method that utilizes design concepts of horizontal stiffener method and RBS and complements their shortcomings.

2.1. Non-scallop welding method

Non-scallop welding method does not keep scallop when connecting beam member and column member for the purpose of relieving strain at the end of beam member, and for the flange part, the method performs glove welds with a backup-bar, and then removes the backup-bar and

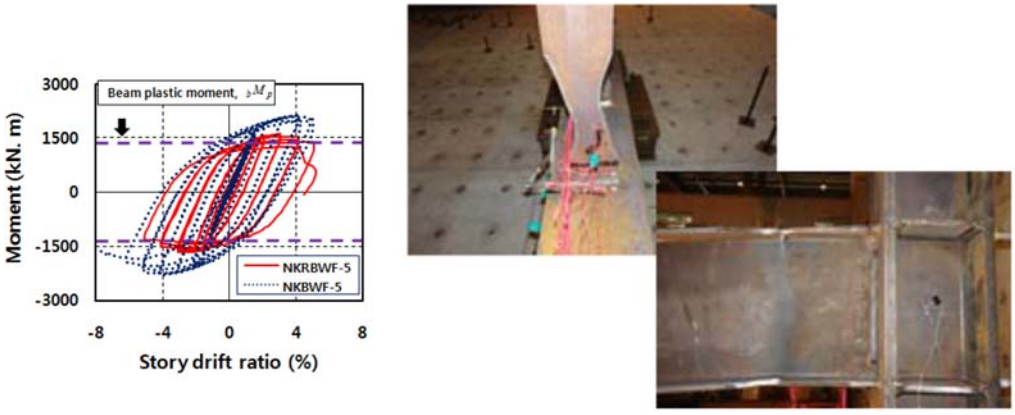

(a) Bearing force degradation (b) Early lateral buckling & fracture

Figure 1. Problems of Reduced Beam Section (Oh *et al*., 2010).

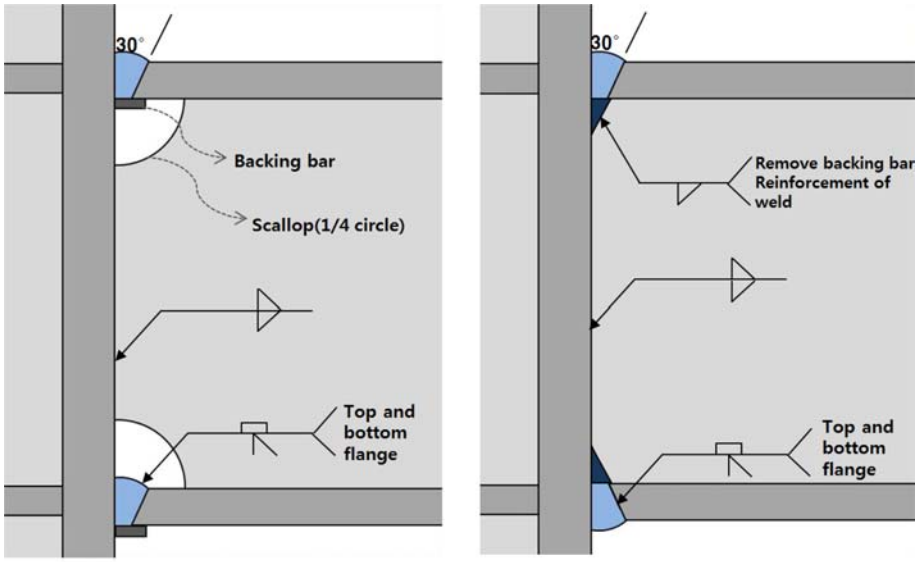

(a) Scallop welding method (b) Non-scallop welding method

Figure 2. Welding Details at Beam End.

reinforces it on the other side of the part by fillet weld, and the web is joined with double-fillet weld. Figure 2 shows comparison of the Non Scallop welding method with the traditional scallop welding method having 1/4 circular scallops. Non-Scallop welding method has an advantage in stress distribution of flange which used to be the major location of brittle fracture in conventional details, as it causes no web partial loss of area at the end of beam. Such an effect has been verified through advanced experimental studies (Oh *et al*., 2010). That is, the studies showed that the deformation capacity of connections was improved as the stress was reduced by beam member in Non-Scallop welding details.

2.2. Improved horizontal stiffener construction method

The improved horizontal stiffener method is the method of adding horizontal steel plate of a unique shape to the upper and lower beam flange, or the lower beam flange. Since this method induces the location of plastic hinge into the beam, it is a method with the same concepts as horizontal stiffener method and RBS which reduce the strain at the end of the beam. However, it is considered as an improved joint method that can sufficiently secure strength and can improve deformation capacity, as it is capable of complementing shortcomings of general horizontal stiffener construction method that can cause stress concentration at the end of stiffener, or those of RBS detail that has the risk of decreased strength and early lateral buckling. The improved horizontal stiffener design will be covered in the next chapter in detail.

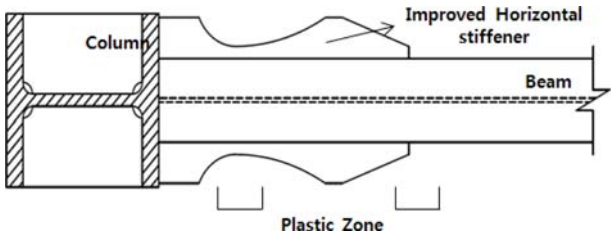

Figure 3. Improved Horizontal Stiffener Construction Method.

3. Improved Horizontal Stiffener Design

In the case of the improved horizontal stiffener method used in this study, plastic hinge can occur at one of the following places depending on design conditions when applying horizontal force: the outer side of column (A section), critical section (The most narrow part of the stiffener: B section), and the end of stiffener part (C section) (Fig. 4). Among them, it is more desirable to have plastic hinge at B or C section rather than A section, where the whole tensile zone belongs to heat-affected zone. In consideration of the above point, the location of flange crop needs to be separated from the outer side of the column by more than a certain distance, and just as RBS design, the extra distance can be calculated by using the following formula (Sign definition: Fig. 5) (Chen, 2001).

$$d_a=(0.5\sim0.75)b_f \quad (1)$$

In addition, it was determined for this study that adjusting B and C section's stress balance to a similar

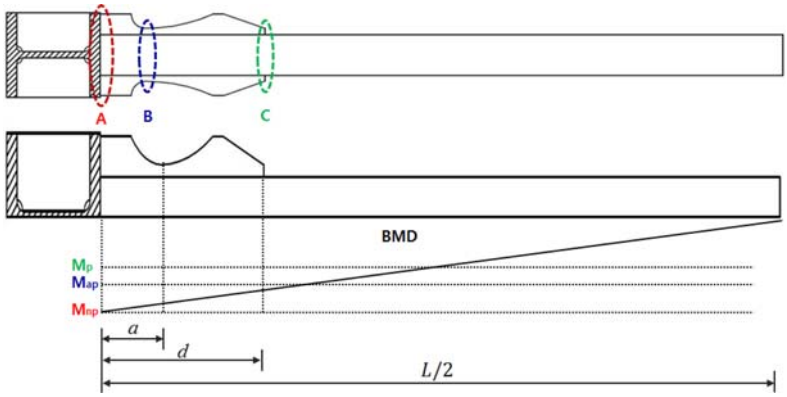

Figure 4. The Moment Gradient for Horizontal Force.

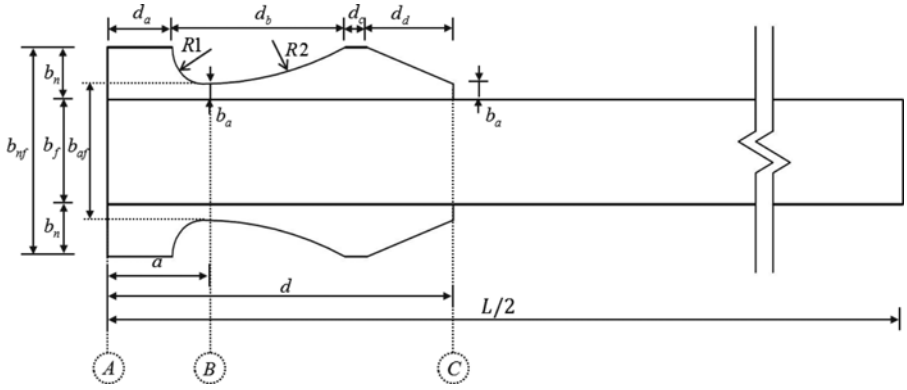

Figure 5. Symbol Definition.

level can help improve deformation capability of the total connections in consideration of the high strength steel's weak deformation capacity. The full plastic moment at each cutting part can be obtained as follows using the basic mechanic formulas.

- The full plastic moment at 'A' crop

$$M_{np} = F_y\left\{(b_{nf}t_f)(h-h_f)+t_f\left(\frac{h}{2}-t_f\right)^2\right\} \tag{2}$$

- The full plastic moment at 'B'

$$M_{ap} = F_y\left\{(b_{af}t_f)(h-h_f)+t_f\left(\frac{h}{2}-t_f\right)^2\right\} \tag{3}$$

- The full plastic moment at 'C'

$$M_p = F_y Z_x \tag{4}$$

where,

F_y: yield strength of material

h: beam depth

Z_x: plastic section modulus of beam

Based on the moment gradient as shown in Fig. 4, the maximum length (d) of horizontal stiffener for preventing plastic hinge at the outer side of column can be defined using the following formula.

$$d = \frac{L}{2M_{np}}(M_{np}-M_p) \tag{5a}$$

where, L: beam span

In addition, the conditions for plastic hinge occurring at B & C section are as follows.

- The condition for plastic hinge first occurring at B section:

$$d > \frac{L}{2}-\frac{M_p}{M_{ap}}\left(\frac{L}{2}-a\right) \tag{5b}$$

- The condition for plastic hinge first occurring at C section:

$$d < \frac{L}{2}-\frac{M_p}{M_{ap}}\left(\frac{L}{2}-a\right) \tag{5c}$$

By considering these two formulas, it is theoretically possible to set the condition for plastic hinge occurring at the B and C section simultaneously by switching the inequality sign with an equality sign, and the optimal variable (X) is defined as follows in this study.

$$X = \frac{M_p}{M_{ap}}\frac{a}{d}+\left(1-\frac{M_p}{M_{ap}}\right)\frac{L}{2d} \tag{6}$$

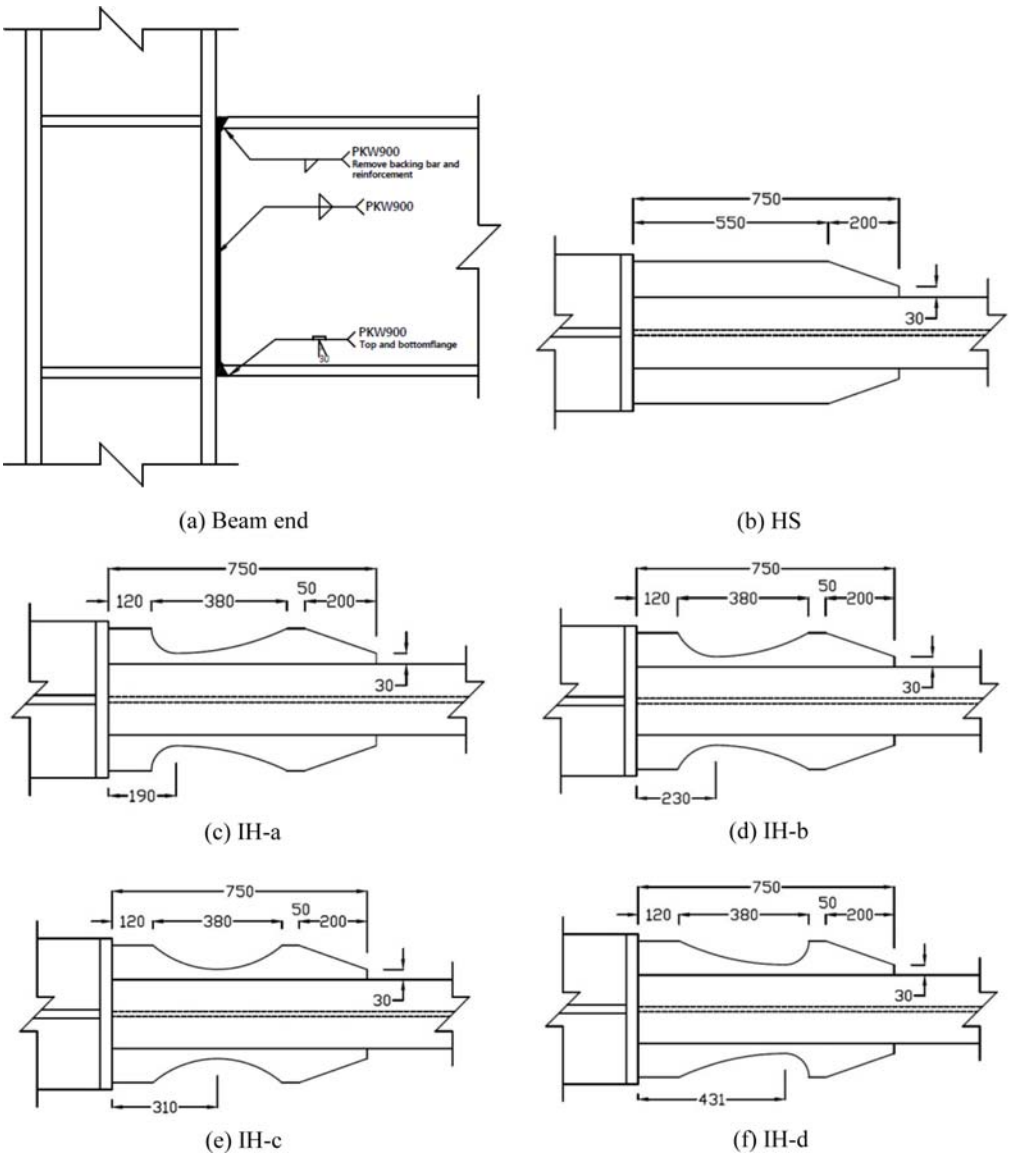

Figure 6. HS, IH series Connection Details.

What it means is that when setting X=1 as a critical point, if it's smaller than 1, then plastic hinge will occur at the B section, and if it's bigger than 1, then plastic hinge will occur at the C section. When applying the practical improved horizontal stiffener construction method, weld beads will be added due to welding at the end of the stiffener, and considering this, the optimal design value of X will be set at a value slightly bigger than 1.

4. Structural Performance Evaluation Test

4.1. Specimen plan

The shape of specimen for the cyclic loading test was the column-tree type beam-to-column connection. The beam span (the distance from loading central point to column central point) was set at 3.5m and the materials used for beam and column were high strength steel HSA800. The size of member section was H-600×200×15×25 for all beam members, and H-440×440×25×35 for all column members. Each beam was made up of Built-up beam members, and the flange and web were welded by full penetrated welding using PKW-900 welding rod made in Korea.

The experiment variable was the difference in connection details, which consisted of 7 specimens. That is, it consisted of the following specimens: connection details with conventional 1/4cycle (R=33) scallop (WC), Non-scallop connection detail (NWC), and Non-scallop specimens employing horizontal stiffener (HS) and improved horizontal stiffener (IH). The improved horizontal stiffener specimens were classified into four categories based on the optimizing parameters. The list of specimens across the experimental variables are shown in Table 1, and details of HS and IH series are shown in Fig. 6.

Table 1. List of Specimens

Specimen	Beam member	Column member	Connection type (Beam edge)	Stiffener reinforcing (HS/IH)	Optimizing parameter (X)	Strength ratio		
						Beam	Column	Panel
WC	H-600×200×15×25 (HSA800)	H-440×440×25×35 (HSA800)	Scallop connection	No	-	1	1.76	1.84
NWC			Non-Scallop connection	Yes (HS)	-	1	1.76	1.84
HS				Yes (IH)	-	1	1.46	1.48
IH-a					0.96	1	1.46	1.48
IH-b					1.00	1	1.46	1.48
IH-c					1.08	1	1.46	1.48
IH-d					1.21	1	1.46	1.48

*Connection details (WC: welded connection, NWC: non-scallop welded connection, HS: horizontal stiffener reinforced connection, IH: improved horizontal stiffener reinforced connection)
*Optimizing parameter (a:0.96, b:1.00, c:1.08, d:1.21)

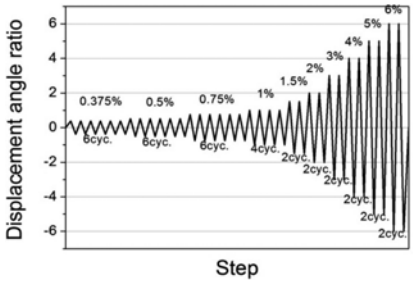

Figure 7. Cyclic Loading Protocol (FEMA 350).

4.2. Test method

As for the boundary conditions for specimens, pinned connections was implemented by fastening the rotary welding jig with the upper and lower part of column using bolts, and repeated hysteresis loading was planned by installing 3,000 kN capacity actuator on the beam member's free end. As for the loading pattern, this study used the cyclic loading protocol on connections as suggested by FEMA350 (Fig. 7). In addition, a confined jig was installed at the place located 700 mm away from the loading point in order to prevent beam member's lateral buckling. The test setup and the scene of test are shown in Figs. 8 and 9.

4.3. Measurement plan

The measurement plans for each connection details are

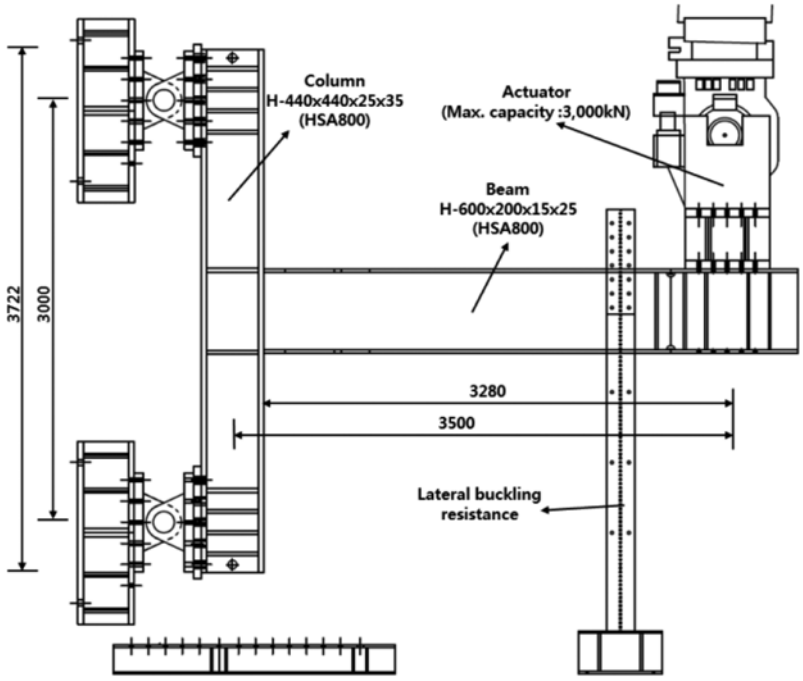

Figure 8. Test Setup.

Figure 9. Scene of Test.

shown in Fig. 10. Strain gauges were attached to 5 sections on the upper and lower flange at equidistant intervals, 3 sections on the web, and 13 sections on the specimen where the horizontal stiffener is not applied. In addition, as for the horizontal stiffener specimen, additional gauges were installed on the locations where plastic hinge is expected, and 2 gauges were added to each end of the stiffener and the critical section of the improved horizontal stiffener. As a result, a total of 30 sections of gauges were attached for general horizontal stiffener specimens and 47 sections of gauges for improved horizontal stiffener specimens.

LVDTs' were installed at a total of 5 places including the same section at the opposition side of the loading point for displacement measurement, 2 sections for displacement measurement at the panel zone, and 2 sections for column displacement measurement.

5. Test Results

5.1. Material tensile test result

The characteristics of material used in this study are shown in Fig. 11 and Table 2. The yield strength was measured with the 0.2% off-set method in consideration of the vague yield point due to the characteristic of high strength steel. The modulus of elasticity showed numerical values similar to the general steel's modulus of elasticity (2×10^5 MPa) And the yield ratio was 0.83, which shows the characteristic of smaller strength increase after yield compared with general structural steel.

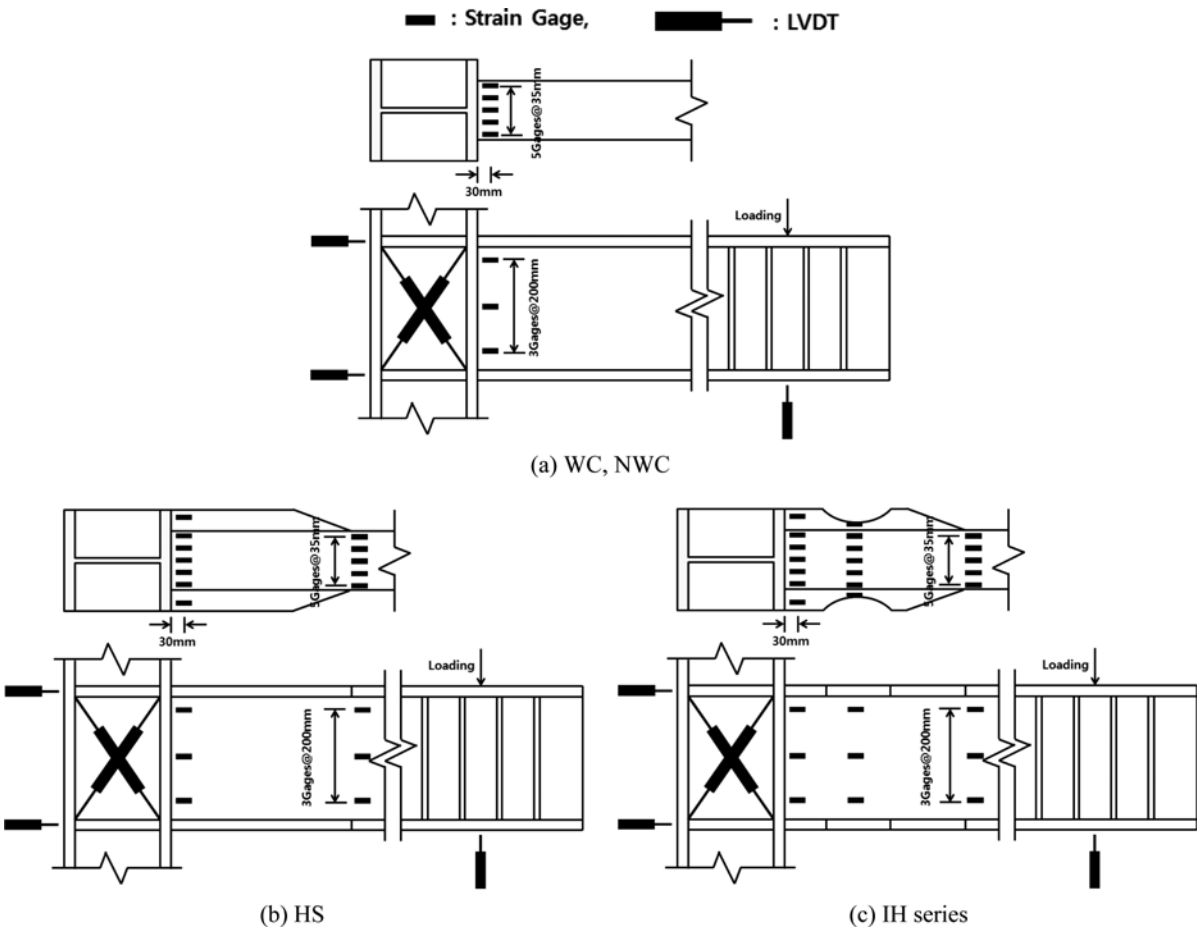

Figure 10. Measurement Plan.

Table 2. Material Characteristics (HSA800)

Steel	Specimen	Young's Modulus E (MPa)	Yield Strength σ_y (MPa)	Tensile Strength σ_u (MPa)	Elongation (%)	Yield Ratio σ_y/σ_u
HSA800	Target	-	650~770	800~950	More than 15	0.85 or less
	No.1	220308	740.6	887.1	22	0.835
	No.2	213831	739.0	888.9	20	0.831
	No.3	199959	739.1	884.5	21	0.836

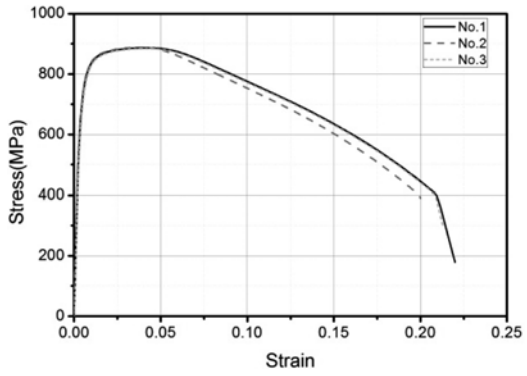

Figure 11. Stress-Strain Relationships (HSA800).

5.2. Connections test result

The moment-rotation angle relationship based on the experiment result is shown in Fig. 12. The horizontal broken line on the graph indicates a beam's full plastic moment and the 80% point of the full plastic moment. In addition, the ultimate conditions of each specimen are shown in Fig. 13. The resisting force for all specimens were above the full plastic moment, but the deformation capacity and ultimate behavior differed across connection details. The followings are the major test results.

5.2.1. WC

The value of maximum moments were 3410.8 kN·m (positive), −3503.9 kN·m (negative), respectively. And the value of maximum rotation angle was 0.03rad. Subsequently, when the first cycle of 0.04rad was loaded, brittle fracture occurred at the beam section's lower flange.

5.2.2. NWC

The maximum rotation angle of NWC specimen was 0.04rad. NWC specimen was a connection detail where Non-scallop method was used as the welding method for the end section unlike the WC specimen. It means that the existence of scallop greatly influenced the strain relaxation effect of connection. However, the ultimate situation showed lower beam flange brittle fracture.

5.2.3. HS

The positive and negative direction maximum moment of the HS specimen to which general horizontal stiffener construction method was applied rose 1.2 times compared with the specimen (NWC) to which horizontal stiffener was not applied due to section reinforcement effect, and it appeared that it's possible to secure excellent deformation capacity since the maximum rotation angle reached to 0.06rad. The cause of this seems to be the fact that the strain concentration was relieved on the outer side of column of which all parts belong to heat-affected zone, due to relocation of the maximum stress point into the beam. However, brittle fracture of the upper beam flange of the stiffener's end section occurred at the time of the final behavior, due to relative concentration of stress at the end of the stiffener.

5.2.4. IH-a

The maximum rotation angle was as high as 0.06rad, and the ultimate situation caused by local buckling and lateral buckling occurred at the expected plastic hinge (B section: the narrowest part of the improved horizontal stiffener). The brittle fracture to ultimate behavior did not occur, and the maximum moment showed a result similar to that of HS specimen.

5.2.5. IH-b, IH-c

In these cases, the stress was distributed effectively at the critical plane of crop within the stiffener and the end of stiffener had been expected, and the specimens showed stable hysteresis behavior until the maximum rotation angle increased to 0.06rad. In addition, at the time of the ultimate behavior, the resisting force deterioration caused by tiny crack on the welding part and local buckling at the end of beam flange rose, but the brittle fracture did not occur.

5.2.6. IH-d

The maximum deformation angle of the IH-d specimen was 0.06rad, but local buckling at the end of stiffener and welding part crack occurred earlier than other improved horizontal stiffener specimens, and it was accompanied by decreased resisting force and stiffness. It means that the visible phenomenon induced by stress concentration occurred early due to the narrower stress distribution zone compared with IH-b, IH-c specimens.

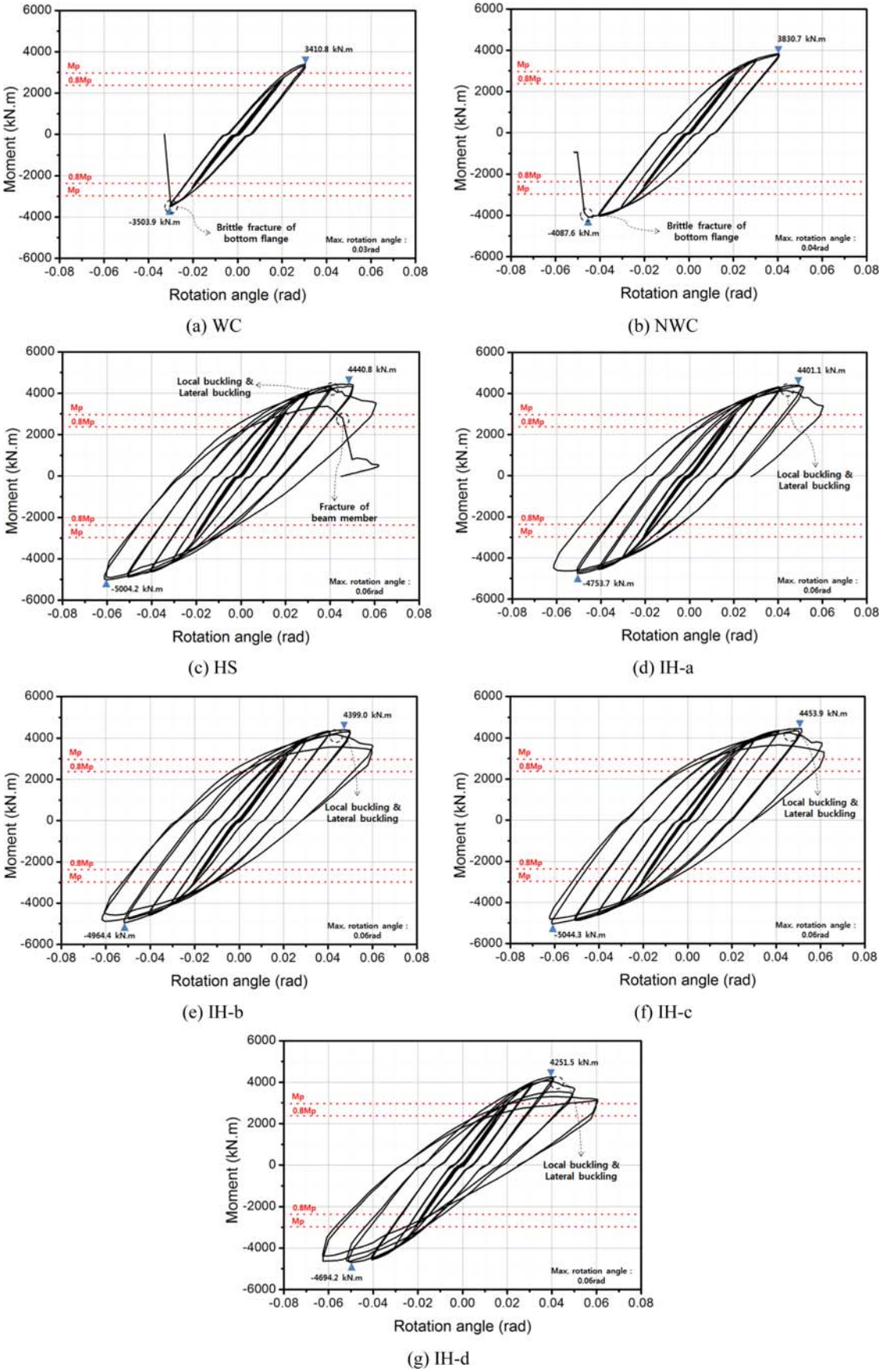

Figure 12. Moment-Rotation Angle Relationships.

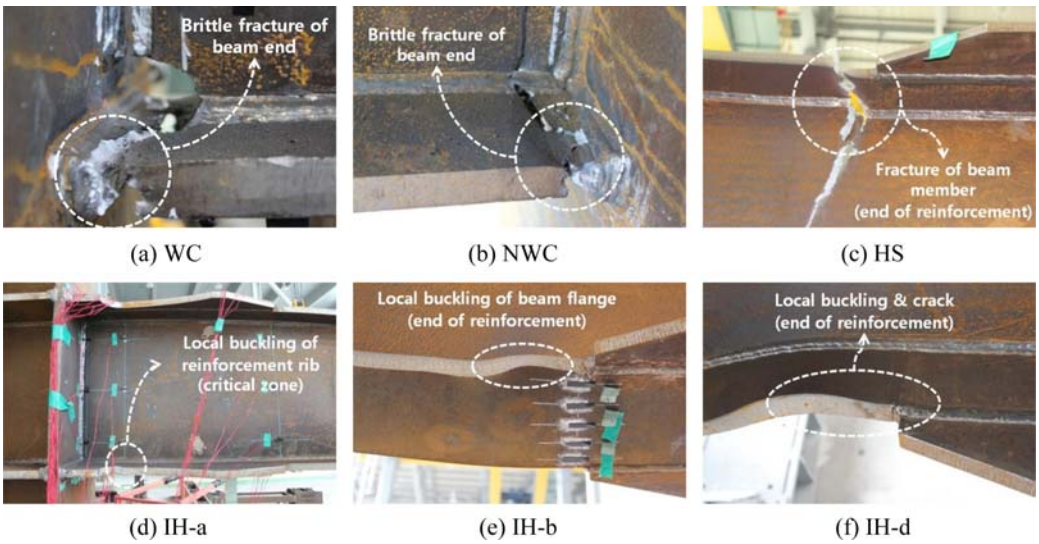

Figure 13. Ultimate Conditions.

Table 3. Structural Performance

Specimen	Loading direction	Initial stiffness (kN/mm)	Yield rotation angle (rad)	Yield moment (kNm)	M_{max} rotation angle (rad)	Maximum moment (kNm)	Maximum rotation angle (rad)	Plastic rotation angle (rad)	Failure mode
WC	Positive (+)	11.24	0.0218	3003	0.0320	3411	0.0320	0.0102	BF
	Negative (-)	11.25	0.0233	3213	0.0296	3504	0.0296	0.0063	
NWC	Positive (+)	11.52	0.0225	3176	0.0415	3831	0.0415	0.0190	BF
	Negative (-)	10.84	0.0262	3476	0.0430	4088	0.0448	0.0186	
HS	Positive (+)	13.36	0.0214	3507	0.0468	4441	0.0622	0.0408	ERF
	Negative (-)	12.82	0.0246	3859	0.0563	5004	0.0577	0.0331	
IH-a	Positive (+)	12.00	0.0238	3504	0.0468	4401	0.0602	0.0364	LB
	Negative (-)	11.67	0.0275	3938	0.0483	4754	0.0590	0.0315	
IH-b	Positive (+)	11.93	0.0226	3308	0.0482	4399	0.0622	0.0396	LB
	Negative (-)	12.62	0.0231	3570	0.0500	4964	0.0604	0.0373	
IH-c	Positive (+)	12.35	0.0231	3501	0.0516	4454	0.0608	0.0377	LB
	Negative (-)	12.54	0.0253	3881	0.0580	5044	0.0580	0.0327	
IH-d	Positive (+)	12.50	0.0226	3456	0.0417	4251	0.0619	0.0393	LB
	Negative (-)	12.35	0.0248	3757	0.0459	4694	0.0582	0.0334	

*BF: brittle failure of beam flange, ERF: end of rib failure, LB: local buckling, and lateral buckling of beam

6. Test Results Analysis

6.1. Skeleton curve

It's necessary to clearly measure yield point for each specimen in order to compare deformation capacity of flexural members. The hysteresis loop caused by repeated loading consists of skeleton curve, Bauschinger, and elastic unloading parts, and among them, the trajectory of the skeleton curve almost corresponded to the load-deformation curve caused by monotonic loading, according to previous researches. In this study, the yield point was measured using the General Yield Point Method after extracting skeleton curves based on the above theories. Major structural performances are defined along with yield points for each specimens in Table 3. What stands out in the Table is that the yield rotation angle of high strength steel was around 0.02rad. It means that the amount of elastic deformation on the high strength steel connections was about twice as bigger, considering that the elastic deformation angle of general mild steel connections was around 0.01rad.

6.2. Deformation capacity of connections

The deformation capacity of connections are schematized

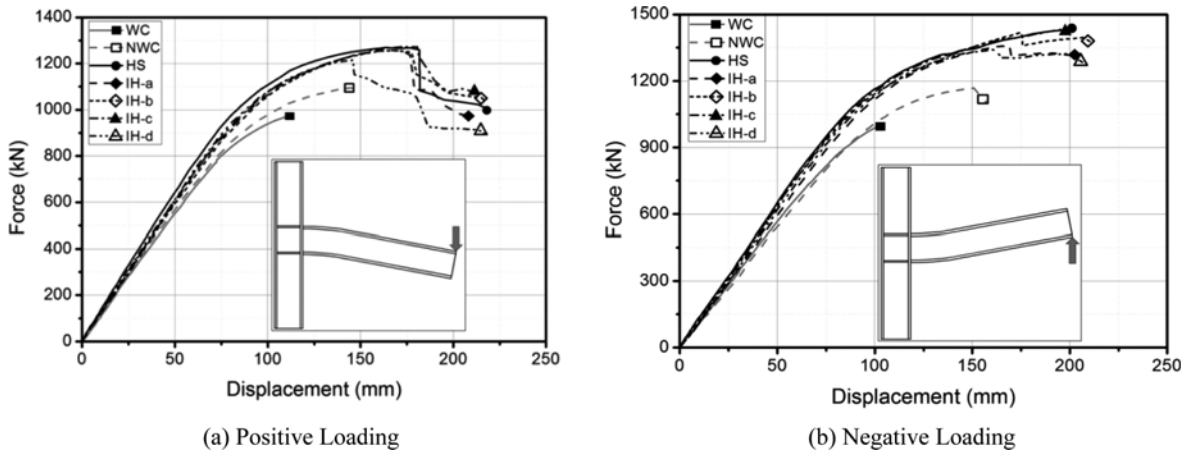

Figure 14. Skeleton Curve.

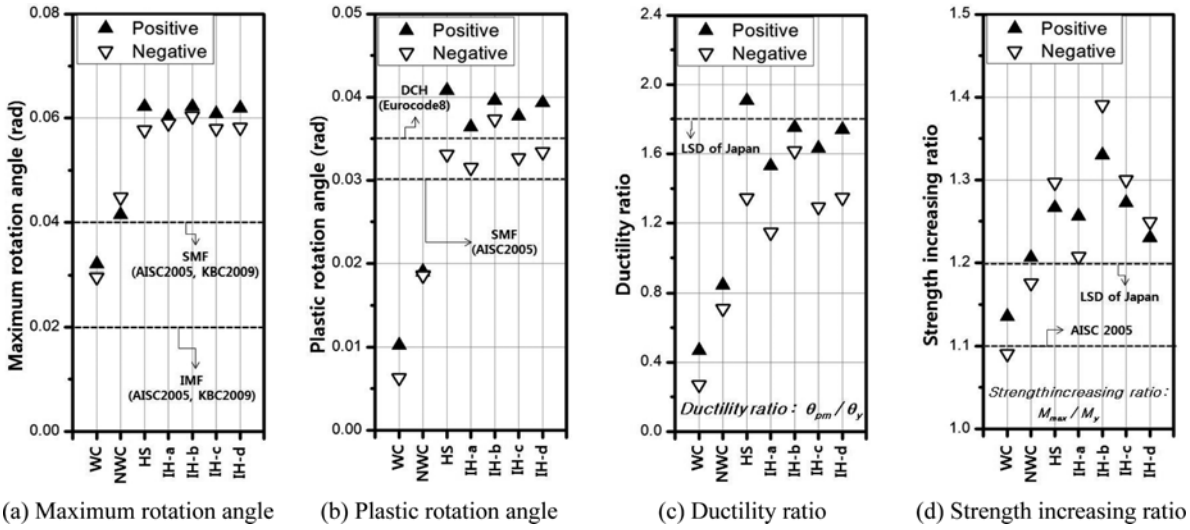

Figure 15. Deformation Capacity.

in Fig. 15 by comparing structural performance of specimens shown in Table 3. Figure 15(a) shows comparison of maximum rotation angles, and the horizontal broken lines indicate the boundary line of the intermediate moment frame (IMF) and special moment frame (SMF) in the AISC2004 and KBC2009 (Korean Building Code 2009) (AISC, 2010; AIK, 2009). As shown in the figure, except for WC, it can be confirmed that 0.04rad rotation angle, which is the requirement of SMF for all specimens, can be secured. Figure 15(b) shows comparison of plastic rotation angle after elastic behavior. Specimens to which general horizontal stiffener and improved horizontal stiffener were applied exceeded the SMF of the AISC criterion and met the plastic rotation angle requirement for high ductility frame specified in Eurocode 8 (AISC, 2010; Eurocode 8, 2003). As mentioned above, the high strength steel frame can secure twice the elastic deformation amount as conventional mild steel frame. Accordingly, there are some disadvantages in terms of ductility ratio, which is defined by dividing the maximum rotation angle by the yield rotation angle. As shown in Fig. 15(c), all specimens showed plastic ratio of less than 1.8, which is the lower limit of plastic ratio for ductility connections suggested in the limit state design proposed in Japan (AIJ, 2001). It is confirmed that strength increasing ratio is more than 1.2 for all specimens except WC specimen (Fig. 15(d)).

6.3. Strain Analysis

6.3.1. Strain of beam end

Figure 16 shows comparison of maximum strains on outer side of column calculated based on the rotation angle. Comparison of tensile strains based on scallop's existence shows that the tensile strain at the beam end of NWC specimen can be reduced to 60% at 0.03rad where WC specimen was destroyed, and it showed that the stress concentration effects on flange caused by partial loss of area caused by scallop was considerably significant. The specimen to which horizontal stiffener was applied showed 85% tensile strain reduction at the 0.03rad rotation angle compared with the WC specimen, and showed 68%

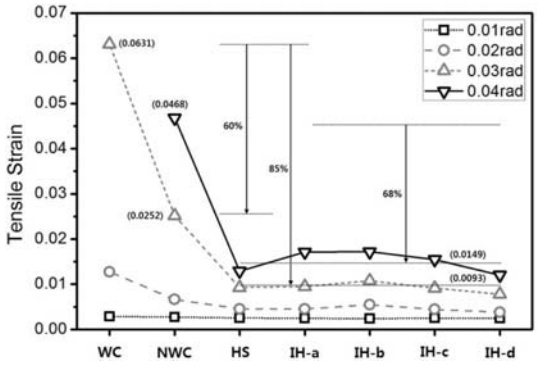

Figure 16. Comparison of maximum strain at the outside of column by specimens.

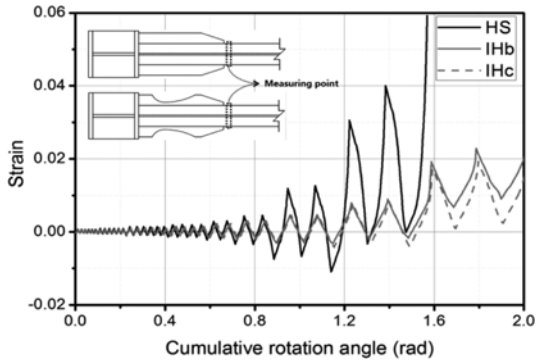

Figure 17. Comparison of deformation angle (HS vs IH) at the end of rib-reinforced area - experiment.

tensile strain reduction at the 0.04rad of rotation angle compared with the NWC specimen. There was no significant difference among the improved horizontal stiffener specimens, but it can be confirmed that the strain at the beam end was increased when the cutting area was closer to outer side of column. The IH-d specimen of improved horizontal stiffener, where the cutting area was located in the most far away area of outer side of column, has the similar plastic hinge rising location compared with the HS specimen to which the general horizontal stiffener was attached, but it seems that the tensile strain at the beam end decreased as the area of stress distribution increased.

6.3.2. General horizontal stiffener vs improved horizontal stiffener

The HS specimen to which the general horizontal stiffener construction method was applied showed comparable performance in terms of connection deformation capacity compared with IH-b and IH-c to which the improved horizontal stiffener was applied, but the brittle behavior could be confirmed in comparison with IH models under the ultimate situation. In order to verify this, we compared the strain of the maximum stress points at the end of the stiffeners of HS, IH-B, IH-c specimens. The result is

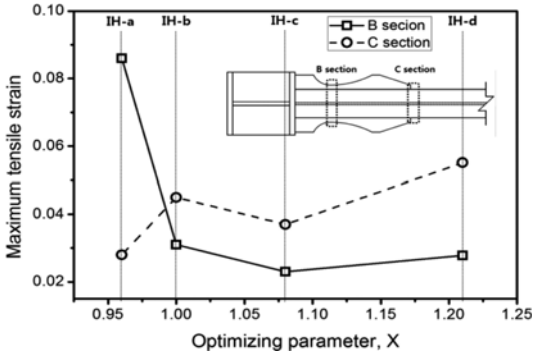

Figure 18. Comparison of maximum tensile strain at the B, C section in IH model.

summarized in Fig. 17. As shown in Fig 17, the strain at the end of stiffener shows a reducing trend due to the stress balancing with the stress concentration section (B section) within the stiffener. As a result, it seems that the problem of stress concentration at the end of the stiffener - which has been pointed out as a structural defect of general horizontal stiffener - can be overcome using the improved horizontal stiffener.

6.3.3. Improved horizontal stiffener optimization review

The purpose of using improved horizontal stiffener lies in dividing the stress concentration into two sections, and distributing the strain at the maximum stress point through stress balance between the two stress concentration sections. It was confirmed that specimens produced by proper design scope by considering stress balance showed generally more stable hysteresis behavior as decrease of resisting force and stiffness after yield of connection occurred at a later point compared with specimens designed out of the optimal design scope. Figure 18 is the schematization result of the maximum tensile strain from B, C section of the improved horizontal specimens at the equal accumulated rotation angle (accumulated rotation angle: 2) against the optimizing parameter (X). The IH-b and IH-c specimens with optimizing parameter of 1 and 1.08 have smaller maximum tensile strain compared with the IH-a and IH-d specimens, and it was confirmed the small difference of tensile strain at the B and C section. Such structural performance of the improved horizontal stiffener constructional method can be effectively applied to flexural member, which may have weak deformation capacity due to high strengthening of welding and materials.

6.4. Energy absorption

The absorptive energy for each specimens were divided into the skeleton part and the Bauschinger part and the result is shown in Fig. 19. The NWC specimen to which the non-scallop construction method was applied showed high values in terms of energy absorption amount at the

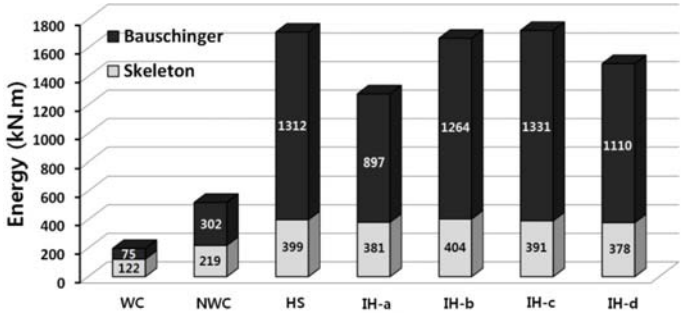

Figure 19. Accumulated Energy Absorption.

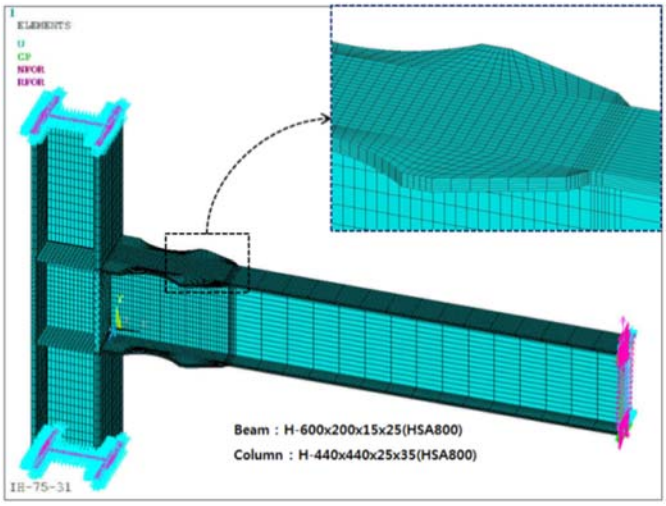

Figure 20. Analysis Model (IH-c).

skeleton part and the Bauschinger part, compared with the WC specimen to which the existing scallop method was applied. The specimen to which the horizontal stiffener was applied showed better energy absorption capacity, and especially, as the deformation capacity in the plastic region improved, the energy absorption amount of the Bauschinger part greatly increased. The specimen to which the improved horizontal stiffener was applied showed similar energy absorption amount at the skeleton part based on the optimizing parameter, but the optimal model specimens showed 14~48% higher absorptive energy at the Bauschinger part due to relatively early deterioration of resisting force and stiffness in non-optimization model specimens.

7. FEM Analysis

7.1. Analysis Method

For the nonlinear finite element analysis, the ANSYS program was used (ANSYS, 2011). The finite element model used Solid185, which is suitable for 3D modeling. The Solid185 element has three directional freedom, and consists of a total of 8 nodes, and it is capable of material and geometrical nonlinear analysis to efficiently reflect the characteristics of steel. The material properties of steel was calculated by substituting the true stress-log strain for HSA800 steel material properties described in Fig. 11 and Table 2. 0.3 poisson's ratio and von-Mises yield theory were applied. In the analysis model, among seven specimens, six specimens except WC specimen were modeled into the real section size. The length of beam was set at 3.5 m, which is the same length used in the test. As for boundary conditions, it was confirmed that all specimens had the weak beam mechanism. and the upper and lower sections of the column members were constrained in three directions (the column members were made to be shorter than in the actual test, so as to reduce the time required for interpretation), and the upward forced displacement from the free end of the beam was applied up to 200 mm (≒0.057rad). The size of mesh at the major strain concentration point was set at the same size (10×10 mm) regardless of analysis variable. The mesh shape and boundary condition of IH-c, the representative analysis model, are shown in Fig 20.

7.2. FEM Analysis Result

The moment-rotation angle relationship based on the analysis result was compared with the test result. The result is shown in Fig. 21. And Table 4 shows the major structural performance. As for the initial stiffness, the analysis results with the ideal conditions was larger compared

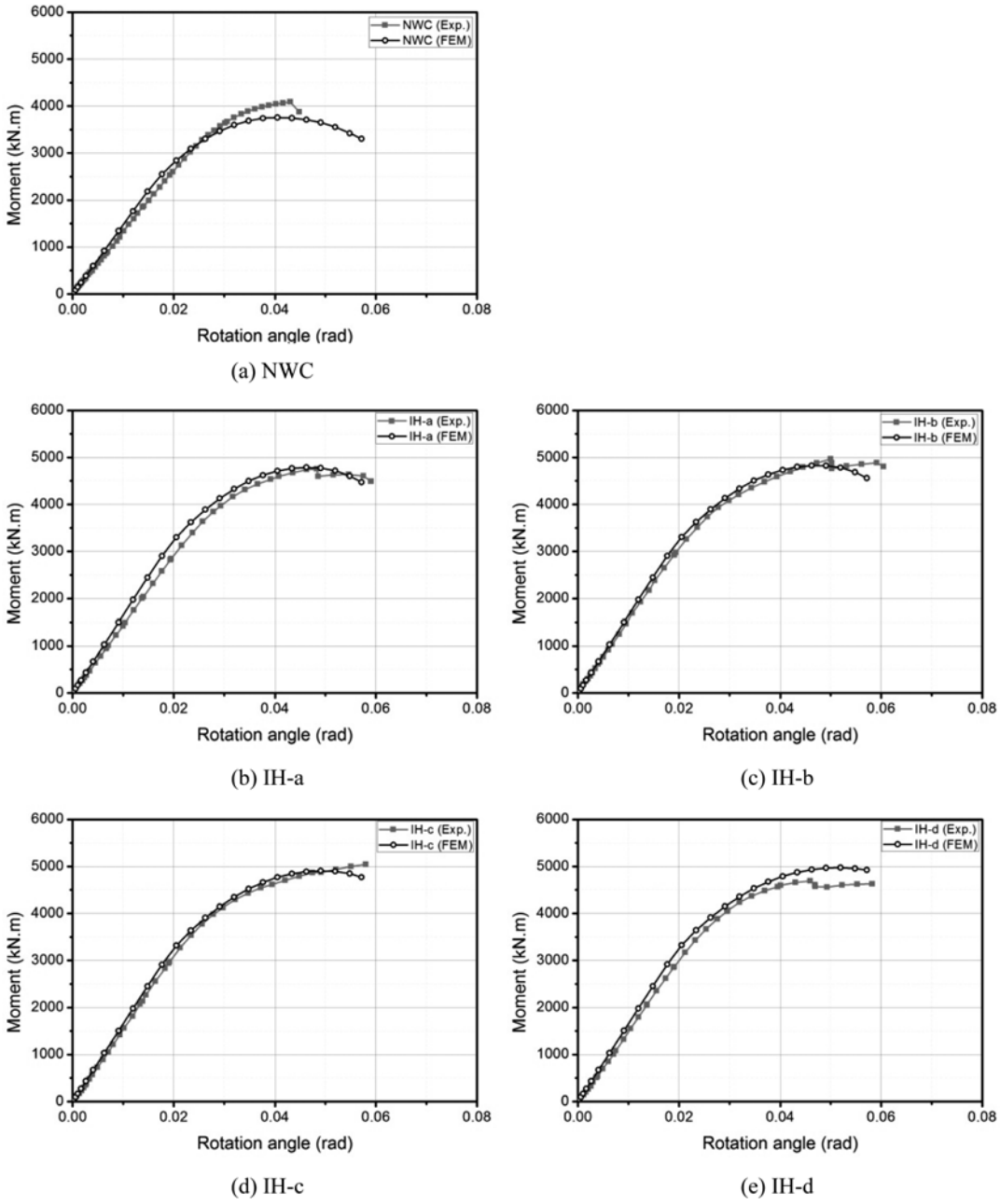

Figure 21. Comparison of Test and Analysis Result.

with the experiment result, but they showed similar responses within the allowable range. The yield moment and maximum moment showed only a slight difference within 10%, and the moment deterioration point (rotation angle at maximum moment) also showed the similar response. Therefore, this model is capable of representing the behaviors from initial deformation, inelastic region to ultimate behavior, and it seems possible to perform a comparative analysis and multi-variable analysis against general structural steel connections without economical and spatial constraints in the future.

Figure 22 shows the von-Mises stress distribution of the major analysis model at 0.03rad rotation angle after connection yield, and as shown in the picture, the stress was concentrated at the end of the beam member in the NWC model, but it can be verified that the stress was evenly distributed within the stiffener's critical section and the end of stiffener in the IH-b model.

7.3. Strain Analysis

The strain reduction effect at the beam end and the stress balance effect, drawn from the analysis result using the same method used in the test result, was schematized as shown in Figs. 23 and 24. The measurement points are the same: drift control point with the rotation angle of 0.04rad. Figure 23 shows that the improved horizontal

Table 4. FEM Analysis Results

Specimen	Method and Error	Initial stiffness (kN/mm)	Yield moment (kNm)	M_{max} rotation angle (rad)	Maximum moment (kNm)
NWC	Exp.	10.84	3476	0.0430	4088
	FEM	12.07	3150	0.0405	3757
	Error (%)	11.3%	9.4%	5.8%	8.1%
IH-a	Exp.	11.67	3938	0.0483	4754
	FEM	13.49	3927	0.0462	4788
	Error (%)	15.6%	2.8%	4.3%	0.7%
IH-b	Exp.	12.62	3570	0.0500	4964
	FEM	13.51	3885	0.0462	4827
	Error (%)	7.1%	8.8%	7.6%	2.8%
IH-c	Exp.	12.54	3881	0.0580	5044
	FEM	13.53	3901	0.0491	4907
	Error (%)	7.9%	0.5%	15.3%	2.7%
IH-d	Exp.	12.35	3757	0.0459	4694
	FEM	13.54	3890	0.0519	4975
	Error (%)	9.6%	3.5%	13.1%	6.0%

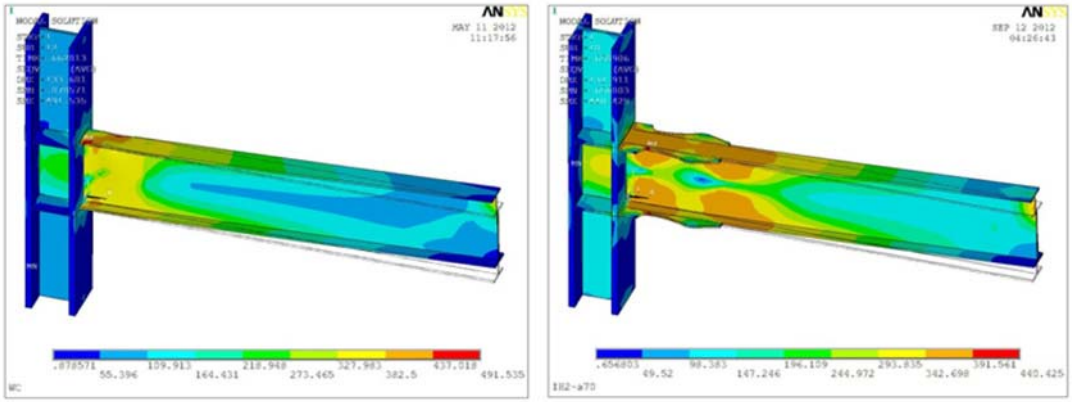

(a) NWC (b) IH-b

Figure 22. Comparison of Stress Distribution (von-Mises Stress Distribution).

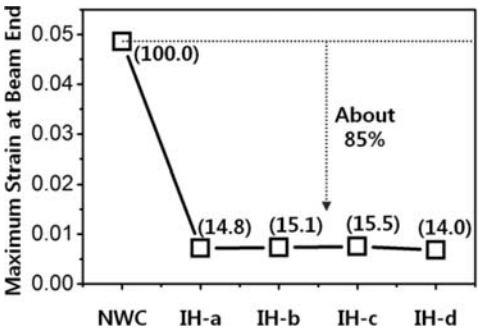

Figure 23. Maximum Strain at Beam End.

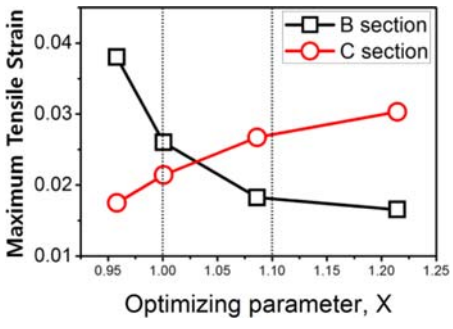

Figure 24. Maximum Tensile Strain Distribution at B, C sections according to Optimizing parameter.

stiffener model can reduce 85% of outer side of column's strain compared with the NWC model.

Figure 25 shows the tensile strain distribution at the reinforced end of the general horizontal stiffener model (HS) and the improved horizontal stiffener model (IH-b) based on the analysis result. It can be confirmed that the strain at the end of stiffener can be greatly relieved compared

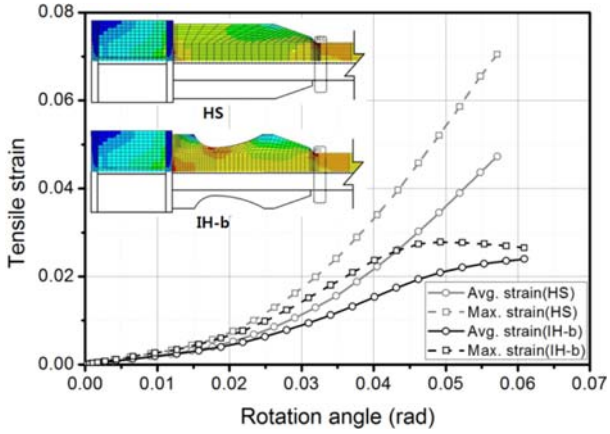

Figure 25. Strain Comparison at the end of Stiffener (HS vs IH)-FEM Result.

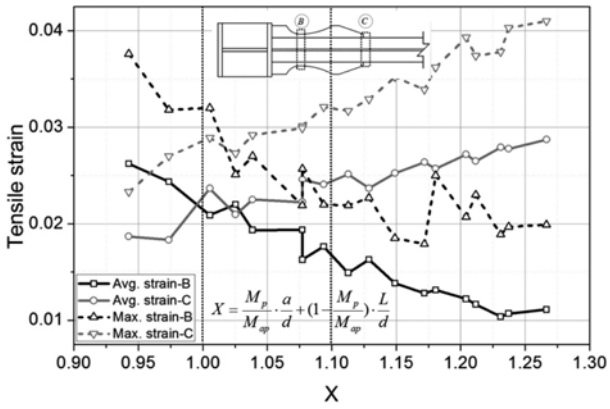

Figure 26. Tensile Strain Distribution on B, C Sections according to optimizing parameters.

with the general horizontal stiffener when using improved horizontal stiffener as was the case in the test result, and the tensile strain was around 0.03 up to the maximum deformation point (≒0.06rad).

7.4. Deduction of the optimal design range for improved horizontal stiffener

In this analysis model, the thickness of weld beards located at the end of the stiffener was modeled with the same size (30 mm) as the margin length (b_a) for welding at the end of the horizontal stiffener, and it's quite likely that the real thickness of weld beards is smaller than the thickness applied in this study. It was confirmed that the IH-b (X=1.00), IH-c (X=1.08) model demonstrated the best stress balance between the B and C section, according to the test result (Fig. 18) and FEM analysis result (Fig. 24) described above. More variable analyses were conducted by applying the material property of the conventional mild steel (SM490) targeting analysis models with confirmed reliability. The tensile strain distribution between B and C at rotation angle of 0.04rad based on the analysis result is shown in Fig. 26.

As was the case in the test and analysis results above, the strain of B and C sections similar value when the optimizing parameter (X) is within the range of between 1.0~1.1, and it's confirmed that the stress is balanced within the expected optimizing parameter range regardless of steel's strength.

As a result, if the material toughness is deficient as in high strength steel, then the improved horizontal stiffener construction method can be applied in order to effectively relieve strain at the connection maximum stress point, and the length (d) of improved horizontal stiffener can be designed with the following range to ensure occurrence of double-plastic hinge within the beam through stress balance.

$$\frac{L}{2}-\left(\frac{M_{ap}}{M_p}\right)\left(\frac{L}{2}-a\right)<d<\frac{L}{2}-\left(\frac{M_p}{M_{np}}\right)\frac{L}{2}$$

In addition, the distance (a) to crop critical plane within the improved horizontal stiffener from the outer side of column can be defined by the following formula.

$$a=\frac{L}{2}-\left\{\frac{L}{2}-(1.0\sim1.1)d\right\}\frac{M_{ap}}{M_p}$$

Here, the improved horizontal stiffener's shape variables d and a are mutually related, and they can be flexibly defined based on the section of beam and column applied in the actual construction.

8. Conclusion

This study considered connection details in order to improve deformation capacity of beam-to-column connection made of high strength steel with high yield ratio. Non-scallop construction method was applied in order to relieve strain at the beam end, and the improved horizontal stiffener construction method was suggested in order to effective stress distribution within the beam. Full-scale test and FEM analysis were conducted in order to verify structural performance and rage of optimal design of the suggested constructional method, and the results are as follows.

(1) It was confirmed that the elastic deformation amounts of high strength steel connections based on the test result can be twice (≒0.02rad) the deformation amount of the general mild steel connections. The increase of the deformation capacity, resisting force, and toughness of connections was significant in the following order: the horizontal stiffener method detail, the non-scallop welding detail, the traditional scallop detail. In particular, the existing horizontal stiffener detail and the improved horizontal stiffener detail show that they are capable of

satisfying the total rotation angle and plastic rotation angle criteria of domestic and foreign high ductile connections. However, it shows that the ductility ratio was undervalued as the elastic deformation angle increased compared with the conventional general structural steel connections.

(2) It was confirmed that the specimen to which the Non-scallop welding method was applied, and the specimens to which the horizontal stiffener construction method was applied were able to reduce the strain of the beam end by 60% and 85% at the same point (rotation angle: 0.03rad) compared with the specimen to which the conventional scallop welding method.

(3) The aspect of connection deformation capacity of the improved horizontal stiffener construction method was comparable to the conventional horizontal stiffener construction method, but it is capable of preventing brittle fracture by effectively relieving strain concentration at the end of stiffener, which is the part of stress concentration.

(4) The nonlinear FEM analysis result conducted in the same test environment showed a response similar to the test result, and an optimal improved horizontal stiffener design formula was suggested by analyzing strain based on the test result and additional FEM analysis.

(5) The improved horizontal stiffener specimen produced with the optimal design shows a stable hysteresis behavior at plastic region due to relatively late occurrence of stiffness and moment deterioration compared with the specimens produced with the non-optimal design. And the energy absorption amount in the Bauschinger part was found to be higher than the specimens produced by non-optimal design by 14~48%.

The results of this study are determined to be able to provide the basic data to establish design criteria for high strength steel beam-to-column connections, and additional test research and analysis studies are needed.

Acknowledgment

This research is supported by a grant from High-Tech Urban Development Program funded by the Ministry of land, transport and maritime affairs.

References

AIJ (2001). *Design guide on steel structures.* Architectural Institude of Japan.

AIK (2009). *Korea building code and commentary-structural*, Architectural Institute of Korea.

AISC (2010). *Specification for structural steel buildings.* American Institute of Steel Construction, USA.

ANSYS (2011). *ANSYS multiphysics, Version 13.0*, ANSYS Inc. Canonsburg, PA, USA.

Bjorhovde, R. (2004). "Development and use of high performance steel." *Journal of Constructional Steel Research*, 60, pp. 393-400.

Chen, S. J. (2001). "Design of ductile seismic moment connections, increased beam section method and reduced beam section method." *International Journal of Steel Structure*, 1(1), pp. 44-52.

Engelhardt, M. D., Fry, G. T., Jones, S., Venti, M., and Holiday, S. (2000). Behavior and design of radius-cut, reduced beam section connections. *SAC Background Document SAC/BD-00/17*, SAC Joint Venture, Richmod, CA.

Eurocode 8 (2005). *Eurocode 8: design provisions for earthquake resistance of structures.-part 1:* general rules, seismic actions and rules for building. EN 1998-1. European Committee for Standardization, Brussels.

Galambos, T. V., Hajjar, J. F., and Earls, C. J. (1997). "Required properties of high-performance steels." *Report No. NISTIR 6004*, NIST.

Hu, J. W. and Hwang, W. S. (2013). "Design and Behavior of recentering Beam-to-CFT column connections with super-elastic shape memory alloy fasteners." *International Journal of Steel Structures*, 13(1), pp. 55-69.

Kim, Y. J. and Oh, S. H. (2008). "Seismic retrofit design of RHS column-to-h beam connections." *Journal of Korean Society of Steel Construction*, KSSC, 20(4), pp. 529-537 (in Korean).

Lee, C. H. and Kim, J. H. (2007). "Seismic design of reduced beam section steel moment connections with bolted web attachment." *Journal of Constructional Steel Research*, 63(4), pp. 522-531.

McDermott, J. F. (1969). "Plastic bending of A514 steel beams." *Journal of Structural Division*, ASCE, 95(ST9), pp. 1851-1871.

Oh, S. H. and Kim, Y. J. (2008). "Analytical study for seismic retrofit of SMRFs connections." *Journal of Korean Society of Steel Construction*, KSSC, 20(3), pp. 445-454 (in Korean).

Oh, S. H., Choi, Y. J., Yoon, S. K., and Lee, D. G. (2010). "Evaluating Seismic Performance of Steel Welded Moment Connections Fabricated with SN Steel." *Journal of Korean Society of Steel Construction*, KSSC, 22(3), pp.271-280 (in Korean).

SAC Joint Venture (2000). Recommended seismic design criteria for new steel moment-frame buildings. *FEMA-350*.

Sophianopoulos, D. S. and Deri, A. E. (2011). "Parameter affecting response and design of steel moment frame reduced beam section connections: an overview." *International Journal of Steel Structures*, 11(2), pp. 133-144.

Uang, C. M. and Bondad, D. (1996a). Dynamic testing of pre-northridge and haunch repaired steel moment connections. *Report No. SSRP-96/03 (Final Report to NSF)*, Univ. of California, San Diego, Calif.

Uang, C. M. and Bondad, D. (1996b). Static cyclic testing of pre-northridge and haunch repaired steel moment connections. *Report No. SSRP-96/02(Final Report to SAC)*, Univ. of California, San Diego, Calif.

Wang, Y., Zhou, H., Shi, Y., and Chen, H. (2010). "Fracture bebavior analyses of welded beam-to-column connections based on elastic and inelastic fracture mechanics." *International Journal of Steel Structures*, 10(3), pp. 253-265.